LETTER

doi:10.1038/nature10791

A novel sensor to map auxin response and distribution at high spatio–temporal resolution

Géraldine Brunoud[1], Darren M. Wells[2]*, Marina Oliva[1]*, Antoine Larrieu[2,3]*, Vincent Mirabet[1], Amy H. Burrow[4], Tom Beeckman[3], Stefan Kepinski[4], Jan Traas[1], Malcolm J. Bennett[2] & Teva Vernoux[1]

Auxin is a key plant morphogenetic signal[1] but tools to analyse dynamically its distribution and signalling during development are still limited. Auxin perception directly triggers the degradation of Aux/IAA repressor proteins[2–6]. Here we describe a novel Aux/IAA-based auxin signalling sensor termed DII-VENUS that was engineered in the model plant *Arabidopsis thaliana*. The VENUS fast maturing form of yellow fluorescent protein[7] was fused in-frame to the Aux/IAA auxin-interaction domain (termed domain II; DII)[5] and expressed under a constitutive promoter. We initially show that DII-VENUS abundance is dependent on auxin, its TIR1/AFBs co-receptors[4–6,8] and proteasome activities. Next, we demonstrate that DII-VENUS provides a map of relative auxin distribution at cellular resolution in different tissues. DII-VENUS is also rapidly degraded in response to auxin and we used it to visualize dynamic changes in cellular auxin distribution successfully during two developmental responses, the root gravitropic response and lateral organ production at the shoot apex. Our results illustrate the value of developing response input sensors such as DII-VENUS to provide high-resolution spatio-temporal information about hormone distribution and response during plant growth and development.

Central to auxin signalling is the ubiquitin- and proteasome-dependent degradation of Aux/IAA catalysed by the SCF-type E3 ubiquitin-ligase complexes $SCF^{TIR1/AFB1-5}$ (refs 2–6, 8). Aux/IAA repressors form heterodimers with transcription factors termed auxin response factors (ARFs)[9,10]. Auxin directly promotes the interaction between TIR1/AFBs auxin co-receptors and Aux/IAAs[5], thus recruiting Aux/IAAs to the SCF complex[3,6] and derepressing ARF-bound loci. This allows the transcription of target genes including most *Aux/IAA* genes, hence providing a negative feedback loop (Fig. 1a)[2,10]. The most widely used tools to monitor auxin distribution *in planta* are *DR5*-based auxin-inducible reporters whose promoter contains several ARF binding sites[11,12]. However, as an output of the auxin response pathway (Fig. 1a), reporter activity does not directly relate to endogenous auxin abundance but also reflects the contribution of a complex signalling pathway[2].

Monitoring the degradation of an Aux/IAA-based green fluorescent protein (GFP) reporter would provide a better target for an auxin sensor as its signal can be related more directly to hormone abundance (Fig. 1a)[3,5,6,13]. This has proved very challenging because Aux/IAA half-lives are often shorter than GFP maturation time[7,14–17]. To overcome this technical limitation, we fused the VENUS fast maturing yellow fluorescent protein (YFP)[7] to the auxin-interaction domain (termed domain II; DII)[5] from several Aux/IAA proteins and expressed these fusion proteins under the constitutive 35S promoter (Fig. 1b and Supplementary Fig. 1a, b). Confocal imaging of transgenic root apical tissues revealed similar fluorescence patterns but the strongest signal

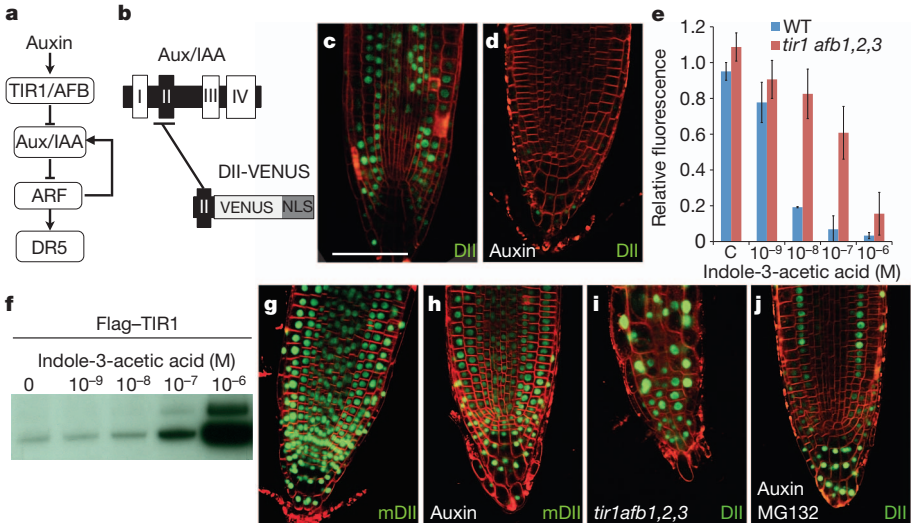

Figure 1 | DII-VENUS degradation is dependent on auxin, TIR1/AFBs and proteasome activity. **a**, Schematic representation of auxin signalling. **b**, Design of DII-VENUS; NLS, nuclear localization signal. **c**, **d**, DII-VENUS fluorescence in absence (**c**) or presence (**d**) of 1 μM indole-3-acetic acid. **e**, Dose-dependent degradation of DII-VENUS in wild-type and mutant roots. **f**, IAA28 domain II peptide pull-down assay with Flag–TIR1 in the presence of indole-3-acetic acid. **g**, **h**, mDII-VENUS fluorescence in the absence (**g**) or presence (**h**) of 1 μM indole-3-acetic acid. **i**, DII-VENUS signal in co-receptor quadruple mutant. **j**, DII-VENUS signal upon 1 μM indole-3-acetic acid and proteasome inhibitor (MG132) co-treatment. Green channel, VENUS; red channel, FM4-64. Scale bar, 50 μm. Error bars, s.d. (WT, $n = 2$; mutant, $n = 3$).

[1]Laboratoire de Reproduction et Développement des Plantes, CNRS, INRA, ENS Lyon, UCBL, Université de Lyon, 69364 Lyon, France. [2]Centre for Plant Integrative Biology, University of Nottingham, Sutton Bonington LE12 5RD, UK. [3]Department of Plant Systems Biology, VIB, Ghent University, B-9052 Gent, Belgium. [4]Centre for Plant Science, Faculty of Biological Sciences, University of Leeds, Leeds LS2 9JT, UK.

*These authors contributed equally to this work.

was obtained using domain II of the most stable Aux/IAA used, IAA28 (Fig. 1c and Supplementary Fig. 1c–f). We thus focused our analyses on this form of the sensor, henceforth called DII-VENUS.

We tested on root tissues the relationship between auxin, its response components and DII-VENUS in several independent ways. First, the DII-VENUS signal was sensitive in a dose-dependent fashion to exogenous auxin treatment (Fig. 1c–e). Second, the DII peptide interacted with its co-receptors TIR1 (Fig. 1f), AFB1 and AFB5 (ref. 18) in an auxin-dependent manner. Third, introducing a mutation in the domain II sequence of DII-VENUS (mDII-VENUS), that disrupts the interaction between Aux/IAA, auxin and the TIR1/AFBs[5], reduced the differential distribution of fluorescence (Fig. 1g; see below for description of pattern) and blocked its auxin-induced degradation (Fig. 1h). Fourth, DII-VENUS fluorescence was ubiquitously distributed in roots of the most strongly affected *tir1 afb1 afb2 afb3* quadruple mutant[4] (Fig. 1i) and the mutants were significantly less sensitive to auxin treatment (Fig. 1e). Fifth, disruption of ubiquitin-dependent breakdown of Aux/IAA proteins using proteasome inhibitors stabilized DII-VENUS and blocked its auxin-induced degradation (Fig. 1j and Supplementary Fig. 2). We conclude that DII-VENUS abundance is regulated by auxin via its receptors, consistent with the model for Aux/IAA degradation (Fig. 1a)[2]. We also demonstrated that DII-VENUS does not disrupt the activity of the auxin response machinery (Supplementary Fig. 3 and Supplementary Information). Hence, DII-VENUS directly reports, but does not interfere with, the input into the auxin signalling pathway.

We next took advantage of the simple cellular organization of the root apex to quantify the distribution of DII-VENUS fluorescence with cellular definition (Fig. 2a, b and Supplementary Fig. 4). Because the TIR1/AFB1-3 co-receptor distribution shows only limited variations in the root meristem region (except in the root cap; Supplementary Fig. 5a–d)[19], this will confer a homogeneous perception capacity. Hence, the spatial distribution of DII-VENUS fluorescence is likely to represent an inverted auxin distribution map in the root tip. This conclusion is further supported by the more homogeneous fluorescence distribution of mDII-VENUS (Fig. 2c and Supplementary Fig. 6) and by the complementary patterns of DII-VENUS and *DR5::VENUS* expression in the quiescent centre, columella and differentiating xylem cells (Fig. 2d, e)[11,20,21]. However, mDII-VENUS fluorescence distribution suggests a higher 35S promoter activity in the epidermis and cortex in the elongation zone and in the most external root cap cells (Fig. 2c and Supplementary Fig. 6). Lower expression of the TIR/AFBs is also expected to confer a lower sensitivity to auxin in the root cap (Supplementary Fig. 5a–d). In both cases, this will lead to an underestimation of auxin levels by DII-VENUS. Analyses of TIR/AFBs co-receptor distribution and of 35S promoter activity are thus essential to interpret the DII-VENUS pattern.

Even considering these biases (Supplementary Information), DII-VENUS quantification indicates that auxin levels are reproducibly higher in the first two tiers of columella cells and initials, the quiescent centre, the stele initials and early daughters and the differentiating xylem cells (Fig. 2b and Supplementary Fig. 4)[22]. The other cells in the root meristem have lower levels of auxin, with minima observed in the epidermis and cortex, but auxin levels significantly increased close to the start of the elongation zone. This increase occurs closer to the root tip in the epidermis and vasculature compared to the cortex (Fig. 2b). The DII-VENUS fluorescence map thus confirms the local maximum of auxin at the quiescent centre and in the columella cells[11] but also allows visualizing the distribution of auxin in the entire root tip. It also reveals a previously unsuspected auxin accumulation starting at the transition zone between the meristem and the elongation zone. These results are in partial agreement with measurements of auxin concentrations in root tissues obtained after cell sorting[23], the differences being possibly due to the higher resolution achieved using DII-VENUS.

We also detected differential distributions of DII-VENUS fluorescence in the vegetative shoot apical meristem (SAM), in the vascular tissues of the hypocotyl (Fig. 2f, g) and later during development in the inflorescence SAM and young floral meristems (Supplementary Fig. 7a–d)[18]. As in the root, reduced differential expression with mDII-VENUS, partly complementary *DR5::VENUS* patterns and distribution of TIR1/AFB1–3 co-receptors (Fig. 2h, i and Supplementary Fig. 5e–h) indicate that the distribution of DII-VENUS fluorescence is primarily controlled by auxin levels in the shoot apex (Supplementary Information)[18]. DII-VENUS is therefore able to report relative auxin distribution at high spatial resolution in various tissues and developmental stages. In addition, in both root and shoot tissues, DII-VENUS is degraded not only in cells where *DR5* is expressed but also in cells that do not express *DR5* (Figs 1c, 2a–f and Supplementary Fig. 7 and Supplementary Information)[18]. This observation demonstrates that the Aux/IAA-ARF signalling pathway contributes significantly to the definition of the *DR5* expression pattern.

To analyse the temporal resolution of the DII-VENUS sensor, we compared dynamic changes in DII-VENUS and *DR5::VENUS* signals

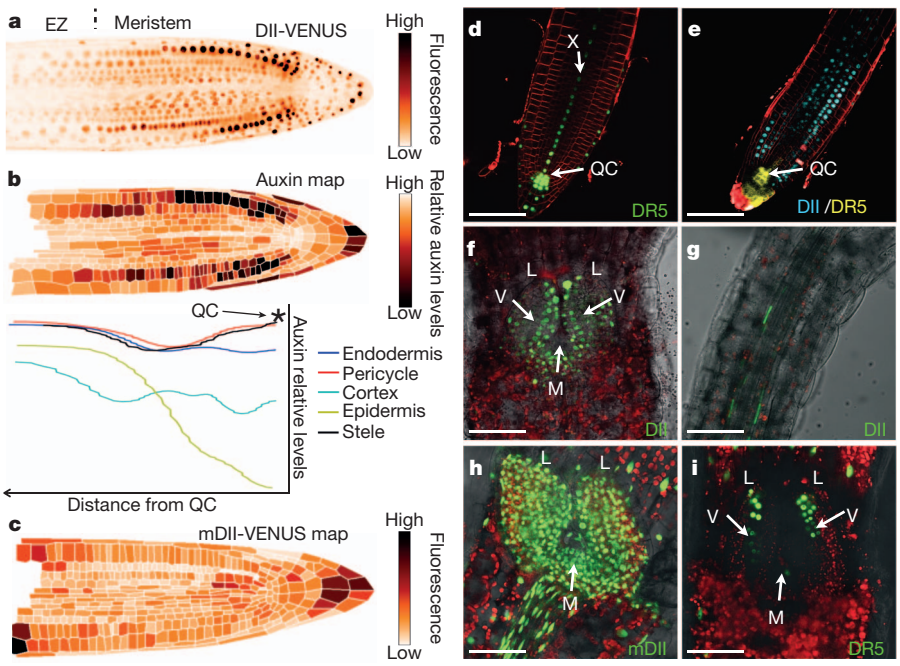

Figure 2 | DII-VENUS provides a sensor to map auxin distribution in plant tissues. **a**–**d**, Root meristematic tissues. **a**, **b**, DII-VENUS fluorescence (**a**) and corresponding map of relative auxin distribution (**b**; top) using the same look-up table. EZ, elongation zone. Tissue-specific changes in auxin levels along the root axis are shown (**b**; bottom). QC, quiescent centre. **c**, Fluorescence map of mDII-VENUS control. **d**, *DR5::VENUS*. X, xylem axis. **e**, DII-VENUS (blue) and *DR5::GFP* (yellow). **f**–**i**, DII-VENUS (**f**, **g**), mDII-VENUS (**h**) and *DR5::VENUS* (**i**) in the vegetative shoot apex (**f**, **h**, **i**) and hypocotyl (**g**). M, meristem; L, leaves; V, vasculature. Green or blue channel, VENUS; yellow channel in **e**, GFP; red channel, FM4-64 (**d**, **e**) or autofluorescence (**f**–**i**). In **f**–**i** the transmission channel has been added. Scale bars, 50 μm.

in roots following exogenous auxin treatment (Fig. 3a, b and Supplementary Movie 1). Time-lapse confocal imaging revealed that the DII-VENUS signal was rapidly lost from all root tissues, whereas the signal in untreated roots remained stable (Fig. 3a and Supplementary Movie 1). Quantification of VENUS fluorescence in the root tip showed that a reduction in the DII-VENUS signal was detected minutes after auxin addition and the signal was abolished within 60 min (Fig. 3b). In contrast, an increase in the *DR5::VENUS* signal was first detected only after 120 min (Fig. 3b). This delay is due to post-transcriptional processes, because quantitative reverse transcription-PCR (qRT–PCR) detected VENUS messenger RNA minutes after auxin treatment (Fig. 3b). We could further show that the DII-VENUS degradation kinetics upon auxin treatment is very similar in different root tissues, but is slower in the root cap (Supplementary Fig. 8). These results indicate similar auxin sensitivity throughout the root except for a lower sensitivity in the root cap, as already suggested by the distribution of the TIR/AFBs (Supplementary Fig. 5a–d). We also observed that the global dynamics of degradation of DII-VENUS was similar in the vegetative and inflorescence SAM, with a minimal fluorescence reached after 1 h (Fig. 3c and Supplementary Fig. 9). We conclude that DII-VENUS responds almost immediately and similarly to exogenous auxin application in various tissues. This observation strengthens our conclusion that DII-VENUS fluorescence is directly related to auxin levels in both shoot and root meristematic tissues but that co-receptor distribution needs to be considered.

Finally, we used DII-VENUS to follow changes in auxin distribution during developmental processes. Roots have been proposed to bend in response to gravity by accumulating auxin on the lower side of root apical tissues[21,24,25]. Consistent with this model, induction of the *DR5* reporter occurs after 1.5–2 h in the lateral root cap (LRC) and epidermis on the lower side of the root (Supplementary Fig. 10)[21]. By contrast, within 30 min of a 90° gravity stimulus the DII-VENUS signal was entirely lost in these tissues on the lower side, whereas fluorescence was stable on the upper side (Fig. 4a). A decrease in DII-VENUS fluorescence was also observed in the cortex and endodermis on both sides of the root and to a lesser extent in vascular tissues. Hence, DII-VENUS

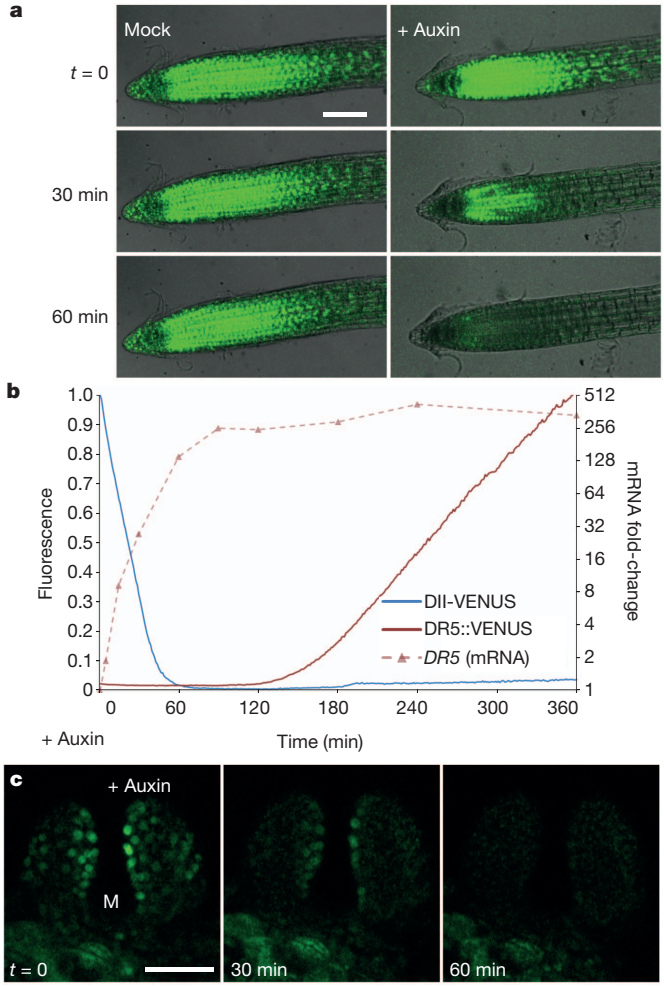

Figure 3 | DII-VENUS monitors changes in auxin response and distribution at high temporal resolution. **a**, Time-course of DII-VENUS fluorescence following either a mock or an auxin treatment (1 μM 1-naphthaleneacetic acid; NAA). **b**, Quantification of DII-VENUS and DR5::VENUS fluorescence and of *DR5::VENUS* mRNA levels in root apices treated with 1 μM NAA. **c**, Time-course of DII-VENUS fluorescence in the shoot apex upon 1 μM indole-3-acetic acid treatment; images are projections of 10 confocal serial sections. Green channel, VENUS. In **a** the transmission channel has been added. Scale bars, 50 μm.

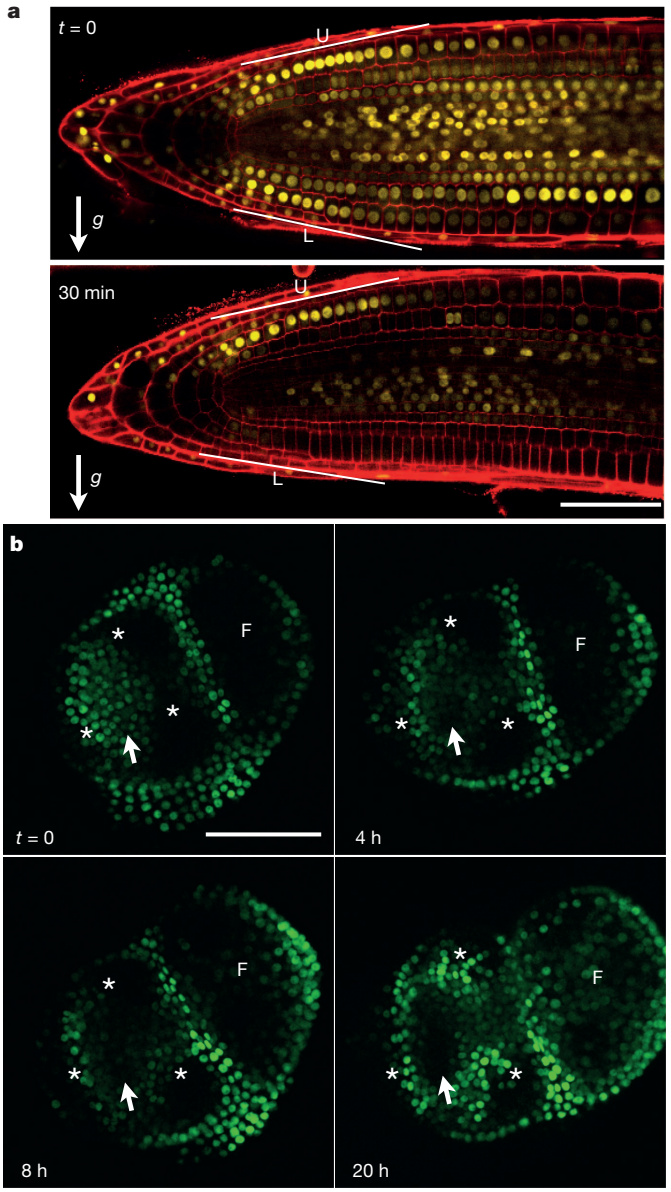

Figure 4 | DII-VENUS allows visualization of changes in auxin distribution during development. **a**, Changes in DII-VENUS fluorescence during a root gravitropic response; *g*, gravity vector; a line was drawn near equivalent cells in the LRC and epidermis on the lower (L) and upper (U) side. **b**, Auxin build-up during organ initiation at the shoot apex visualized using DII-VENUS; arrow, site of new organ initiation; asterisks, groups of nuclei showing notable changes in fluorescence; F, flower. Yellow or green channel, VENUS; red channel, propidium iodide. Scale bars, 50 μm.

indicates that the changes in auxin concentration are not restricted to the LRC and epidermis during the gravitropic response. We next used DII-VENUS to follow auxin-dependent organ initiation at the SAM (Fig. 4b)[26,27]. DII-VENUS allowed the visualization of the progressive build-up of auxin triggering the formation of a new organ (Fig. 4b). It also demonstrated significant redistribution of DII-VENUS fluorescence throughout the SAM, most probably reflecting the dynamics of auxin transport in the tissue[27]. Taken together, our observations demonstrate that, during both shoot and root development, DII-VENUS detects dynamic changes in endogenous auxin distribution and responses that are more complex than previously thought. By demonstrating that DII-VENUS and *DR5* fluorescence patterns are only partly complementary, we also provide evidence that the auxin signalling pathway has a key role in the spatial control of transcription in response to auxin during developmental processes. Finally, several other plant hormones have been shown to signal through degradation of key signalling regulators[28–30]. Our work provides the foundation for building synthetic signalling sensors for different hormones to explore their role during development.

METHODS SUMMARY

Generation and characterization of DII-VENUS reporter plants. Aux/IAA degron sequences[16] were fused to VENUS-NLS under the control of the 35S promoter (Supplementary Fig. 1) and recombined into gateway binary vector pH7m34GW (http://gateway.psb.ugent.be/). Plasmids were transformed into Col-0 plants by floral dipping.

Microscopy, live imaging and chemical treatments. All images were obtained using laser-scanning confocal microscope. Tissue organization was visualized using FM4-64, propidium iodide, transmission or chlorophyll autofluorescence. For live imaging of shoot meristems, plants were grown on the auxin transport inhibitor 1-*N*-naphthylphthalamic acid (NPA) to produce naked apices before transferring to a new medium without NPA. To generate maps of relative auxin distribution in the root meristem, a cellular grid was generated from a median optical section and for each cells fluorescence was extracted from the optical section cutting the nucleus at its most median part.

For analysis of chemically treated roots, 5-day-old DII-VENUS seedlings were transferred to media containing the chemicals at the stated concentration. For root live imaging, immediately following transfer, the seedlings were scanned every 2 to 5 min for 2 h. The fluorescence intensity over identical scanned portion of the root (corresponding approximately to the first 200 μM from the root tip) was extracted at each time point. For tissue-specific kinetics, fluorescence was extracted from groups of nuclei with nearly identical fluorescence in the different tissues. For the vegetative SAM, 5-day-old DII-VENUS seedlings were mounted in water after removing one cotyledon to allow observation of the vegetative shoot apex before treating with the stated concentration of auxin.

Pull-down assays. Pull-down assays were performed using a 35S:Flag-TIR1 line and biotinylated IAA28 peptide. The immunodetection of TIR1/AFB–Flag was performed with a 1:5,000 dilution of anti-Flag 2-peroxidase (HRP) antibody followed by chemiluminescent detection with ECL plus reagents.

Full Methods and any associated references are available in the online version of the paper at www.nature.com/nature.

Received 11 July; accepted 19 December 2011.
Published online 15 January 2012.

1. Friml, J. Auxin transport — shaping the plant. *Curr. Opin. Plant Biol.* **6,** 7–12 (2003).
2. Chapman, E. J. & Estelle, M. Mechanism of auxin-regulated gene expression in plants. *Annu. Rev. Genet.* **43,** 265–285 (2009).
3. Dharmasiri, N., Dharmasiri, S. & Estelle, M. The F-box protein TIR1 is an auxin receptor. *Nature* **435,** 441–445 (2005).
4. Dharmasiri, N. *et al.* Plant development is regulated by a family of auxin receptor F box proteins. *Dev. Cell* **9,** 109–119 (2005).
5. Tan, X. *et al.* Mechanism of auxin perception by the TIR1 ubiquitin ligase. *Nature* **446,** 640–645 (2007).
6. Kepinski, S. & Leyser, O. The *Arabidopsis* F-box protein TIR1 is an auxin receptor. *Nature* **435,** 446–451 (2005).
7. Shaner, N. C., Steinbach, P. A. & Tsien, R. Y. A guide to choosing fluorescent proteins. *Nature Methods* **2,** 905–909 (2005).
8. Greenham, K. *et al.* The AFB4 auxin receptor is a negative regulator of auxin signaling in seedlings. *Curr. Biol.* **21,** 520–525 (2011).
9. Ulmasov, T., Hagen, G. & Guilfoyle, T. J. ARF1, a transcription factor that binds to auxin response elements. *Science* **276,** 1865–1868 (1997).
10. Guilfoyle, T. J. & Hagen, G. Auxin response factors. *Curr. Opin. Plant Biol.* **10,** 453–460 (2007).
11. Sabatini, S. *et al.* An auxin-dependent distal organizer of pattern and polarity in the *Arabidopsis* root. *Cell* **99,** 463–472 (1999).
12. Ulmasov, T., Murfett, J., Hagen, G. & Guilfoyle, T. J. Aux/IAA proteins repress expression of reporter genes containing natural and highly active synthetic auxin response elements. *Plant Cell* **9,** 1963–1971 (1997).
13. Gray, W. M., Kepinski, S., Rouse, D., Leyser, O. & Estelle, M. Auxin regulates SCF^{TIR1}-dependent degradation of AUX/IAA proteins. *Nature* **414,** 271–276 (2001).
14. Ramos, J. A., Zenser, N., Leyser, O. & Callis, J. Rapid degradation of auxin/indoleacetic acid proteins requires conserved amino acids of domain II and is proteasome dependent. *Plant Cell* **13,** 2349–2360 (2001).
15. Zenser, N., Ellsmore, A., Leasure, C. & Callis, J. Auxin modulates the degradation rate of Aux/IAA proteins. *Proc. Natl Acad. Sci. USA* **98,** 11795–11800 (2001).
16. Dreher, K. A., Brown, J., Saw, R. E. & Callis, J. The *Arabidopsis* Aux/IAA protein family has diversified in degradation and auxin responsiveness. *Plant Cell* **18,** 699–714 (2006).
17. Abel, S., Oeller, P. W. & Theologis, A. Early auxin-induced genes encode short-lived nuclear proteins. *Proc. Natl Acad. Sci. USA* **91,** 326–330 (1994).
18. Vernoux, T. *et al.* The auxin signalling network translates dynamic input into robust patterning at the shoot apex. *Mol. Syst. Biol.* **7,** 508 (2011).
19. Parry, G. *et al.* Complex regulation of the TIR1/AFB family of auxin receptors. *Proc. Natl Acad. Sci. USA* **106,** 22540–22545 (2009).
20. Benková, E. *et al.* Local, efflux-dependent auxin gradients as a common module for plant organ formation. *Cell* **115,** 591–602 (2003).
21. Ottenschläger, I. *et al.* Gravity-regulated differential auxin transport from columella to lateral root cap cells. *Proc. Natl Acad. Sci. USA* **100,** 2987–2991 (2003).
22. Santuari, L. *et al.* Positional information by differential endocytosis splits auxin response to drive *Arabidopsis* root meristem growth. *Curr. Biol.* **21,** 1918–1923 (2011).
23. Petersson, S. V. *et al.* An auxin gradient and maximum in the *Arabidopsis* root apex shown by high-resolution cell-specific analysis of IAA distribution and synthesis. *Plant Cell* **21,** 1659–1668 (2009).
24. Boonsirichai, K., Guan, C., Chen, R. & Masson, P. H. Root gravitropism: an experimental tool to investigate basic cellular and molecular processes underlying mechanosensing and signal transmission in plants. *Annu. Rev. Plant Biol.* **53,** 421–447 (2002).
25. Boonsirichai, K., Sedbrook, J. C., Chen, R., Gilroy, S. & Masson, P. H. ALTERED RESPONSE TO GRAVITY is a peripheral membrane protein that modulates gravity-induced cytoplasmic alkalinization and lateral auxin transport in plant statocytes. *Plant Cell* **15,** 2612–2625 (2003).
26. Reinhardt, D. *et al.* Regulation of phyllotaxis by polar auxin transport. *Nature* **426,** 255–260 (2003).
27. Heisler, M. G. *et al.* Patterns of auxin transport and gene expression during primordium development revealed by live imaging of the *Arabidopsis* inflorescence meristem. *Curr. Biol.* **15,** 1899–1911 (2005).
28. Silverstone, A. L. *et al.* Repressing a repressor: gibberellin-induced rapid reduction of the RGA protein in *Arabidopsis*. *Plant Cell* **13,** 1555–1566 (2001).
29. Fu, X. & Harberd, N. P. Auxin promotes *Arabidopsis* root growth by modulating gibberellin response. *Nature* **421,** 740–743 (2003).
30. Santner, A. & Estelle, M. Recent advances and emerging trends in plant hormone signalling. *Nature* **459,** 1071–1078 (2009).

Supplementary Information is linked to the online version of the paper at www.nature.com/nature.

Acknowledgements We thank A. Erktan and C. Cellier for help with marker expression analysis; J. Neve, A. Miyawaki, M. Heisler and M. Estelle for providing the *35S::Flag-TIR1* line, *VENUS* complementary DNA, DR5::VENUS plasmids and TIR/AFB GUS lines, respectively; the PLATIM for access to confocal microscopes; F. Parcy, O. Hamant, A. Boudaoud and P. Das for discussions. T.V. was supported by the Human Frontier Science Program Organization (CDA 0047/2007 HFSPO) and the Agence National de la Recherche (ANR-07-JCJC-0115 and EraSysBio+ iSAM). D.M.W., A.L. and M.J.B. acknowledge the support of the Biotechnology and Biological Sciences Research Council (BBSRC) and Engineering and Physical Sciences Research Council (EPSRC) funding to the Centre for Plant Integrative Biology (CPIB); BBSRC grants BB/F013981/1 and BB/F007418/1 to S.K.; BBSRC Professorial Research Fellowship funding to D.M.W. & M.J.B.; and Belgian Scientific policy (BELSPO contract BARN) to A.L., T.B. and M.J.B.

Author Contributions T.V. designed the DII-VENUS tool. G.B., M.O. and T.V. engineered and characterized DII-VENUS transgenic lines. D.M.W., G.B., A.L. and V.M. quantified the spatial and temporal dynamics of DII-VENUS. A.H.B. did the pull-down assay. T.V. and M.J.B. designed the experiments with the help of T.B., S.K. and J.T. T.V. and M.J.B. analysed the data and wrote the paper. All authors discussed the results and commented on the manuscript.

Author Information Seed for the lines described in this study have been deposited at the Nottingham *Arabidopsis* Stock Centre. Reprints and permissions information is available at www.nature.com/reprints. The authors declare no competing financial interests. Readers are welcome to comment on the online version of this article at www.nature.com/nature. Correspondence and requests for materials should be addressed to T.V. (teva.vernoux@ens-lyon.fr).

METHODS

Plant material, growth conditions and plant treatments. All transgenic plants were generated in the Columbia ecotype (Col-0). The *tir1 afb1 afb2 afb3* quadruple mutant, DR5::GFP line and TIR1/AFB1–AFB3 GUS translational fusions have been described[4,19,31]. *DR5::VENUS* transgenic plants were generated by transforming a *DR5::VENUS* plasmid[27] by floral dipping[32]. Plants were cultivated *in vitro* on MS medium supplemented with 1% sucrose at 22 °C and under long-day conditions (16 h light/8 h darkness). For analysis on roots, the chemical treatments were done on 5-day-old plants by transferring them to liquid MS supplemented with the chemicals or on an MS agar supplemented with the chemicals for root live imaging. Indole-3-acetic acid (Sigma) or 1-naphthaleneacetic acid (NAA; Sigma) was dissolved in ethanol and used at the indicated concentration. MG132 and clasto-lactacystin-β-lactone (lactacystin; Sigma) were dissolved in dimethylsulphoxide (DMSO) and used at the final concentration of 50 μM for 2.5 h or 20 μM for 8 h respectively. For MG132/indole-3-acetic acid co-treatments, plants were pretreated with MG132 for 1.5 h before adding indole-3-acetic acid. For analysis on the vegetative shoot apex, 5-day-old seedlings were used after removing one cotyledon to allow observation of the vegetative shoot apex. Seedlings were mounted in water and treatments were done by replacing by capillarity the water with indole-3-acetic acid at the indicated concentration. For the inflorescence apex, the plants were transferred to water containing indole-3-acetic acid at the indicated concentration.

Generation of DII-VENUS transgenic plants. The DII-VENUS binary vectors were generated using Gateway technology and following the Multisite Gateway three-fragment vector construction kit protocol (Invitrogen). To generate the different versions of the DII-VENUS sensor (Supplementary Fig. 1), we used the region of IAA8, IAA9 and IAA28 starting from the conserved lysine up to the end of domain II (IAA8, amino acid positions 107–178; IAA9, 120–195; IAA28, 28–61; Supplementary Fig. 1). IAA8, IAA9 and IAA28 were chosen because their basal half-lives were potentially long enough[16] (ranging from 15–20 min for IAA8 and IAA9 to 80 min for IAA28) to allow for the maturation of the fast-maturing YFP variant VENUS and thus for visualization of its fluorescence. We cloned the *IAA8*, *IAA9* and *IAA28* cDNAs by standard RT–PCR from inflorescence mRNA. The different wild-type sequences were then amplified by PCR (see Supplementary Table 1 for primers) and cloned in pDONR 221 by recombination. We then mutated the conserved lysine (K to R mutation) by introducing this mutation in the forward primers (sequence in bold replaced by AGA: see Supplementary Table 1). To generate mDII-VENUS, site-directed mutagenesis (using standard inverted PCR procedures) was used to introduce the P53L mutation in the wild-type IAA28 sequence in pDONR 221 (Supplementary Fig. 1)[33]. The sequence of VENUS fused to the N7 nuclear localization signal[34] was amplified by PCR (see Supplementary Table 1 for primers) from a VENUS-N7 sequence cloned in pBG36 and cloned into pDONR P2R-P3 by recombination. Finally Aux/IAA-derived sequences were fused in-frame to VENUS-N7 (Supplementary Fig. 1) and put under the control of the strong constitutive CaMV 35S promoter, using a 35S promoter cloned in pDONR P4-P1R and recombination into the gateway-compatible pH7m34GW binary vector[35] (hygromycin resistance). The different plasmids were then introduced in plants by floral dipping[32].

Confocal microscopy, live imaging and quantification of fluorescence. Imaging was performed either on either a LSM-510 laser-scanning confocal microscope (Zeiss), a SP5 spectral detection confocal microscope (Leica) or an Eclipse Ti 2000 laser-scanning confocal microscope (Nikon). For visualization of the root organization the roots were stained either with FM4-64 (Invitrogen) as previously described[36] or propidium iodide (Sigma). To quantify fluorescence with cellular resolution in DII-VENUS and mDII-VENUS root meristems and generate maps of relative auxin using DII-VENUS, serial optical sections were obtained. A cellular grid was generated from the propidium iodide channel of the most median optical section using Merrysim[37]. For each cell defined in the grid, we then selected the optical section passing through the centre of each nuclei. Fluorescence was then summed inside the corresponding cell from that section. The loss of fluorescence due to tissue absorbance was also estimated using the spatial distribution of the propidium iodide channel and used to correct the fluorescence values. To obtain the changes in auxin levels along the root axis in the different tissues, fluorescence distribution was extracted and curvatures were smoothed using a Gaussian kernel with a sigma value of 5.

For root live imaging, immediately after the beginning of the treatment, the seedlings were scanned every 2 min for 2 h to follow the evolution of the DII-VENUS signal. To quantify fluorescence in the root tip, the average fluorescence intensity over identical scanned portion of the root (corresponding approximately to the first 200 μM from the root tip) was extracted using EZ-C1 software (v3.9, Nikon) and the values analysed using Microsoft Excel. For tissue specific kinetics, the seedlings were scanned every 5 min and fluorescence was extracted from groups of nuclei with nearly identical fluorescence (variations $< 30\%$) in the different tissues. The fluorescence intensity of nuclei was extracted from the different tissues using the ROI tool of Fiji software (http://fiji.sc/wiki/index.php/Fiji) and the values analysed using Microsoft Excel. For dose-dependent quantification of DII-VENUS signal upon auxin treatment, fluorescence was measured 1 h after treatment using two and three roots for wild-type and *tir1 afb1 afb2 afb3*, respectively.

For the vegetative shoot apex, seedlings were mounted into water in between slide and cover slip. For live imaging of vegetative shoot apex, five plants were treated after observation at $t = 0$ and followed over 90 min. For the inflorescence apex, observation was performed as described[38]. Live imaging of the inflorescence apex was performed on plants grown on the auxin transport inhibitor NPA then transferred to a new medium without NPA as previously described[39]. Initiation of a new organ was confirmed a posteriori by visual inspection of the apex.

Root growth analysis, gravitropic assays and flower production rate. For analysis of root growth, plants were grown near-vertically and root length was measured at the indicated time. For gravitropic assays, plants were grown as detailed previously[40] and imaged at 30 min intervals following a 90° gravi-stimulus. Root tip angle was measured using modified RootTrace software[41] (http://www.cpib.ac.uk/tools-resources/roottrace). Estimation of flower production rate was done as described[42].

IAA28–Flag–TIR1 pull-down assays. To generate the *35S::Flag-TIR1* transgenic *Arabidopsis* line a plant expression vector containing a 3×Flag was first created by annealing complementary 101-base-pairs oligonucleotides including the 3×Flag coding sequences (see Supplementary Table 1) and cloning this fragment into XbaI and SalI sites of the vector pFP101. The Gateway C1 cassette (Invitrogen Gateway vector conversion reagent system) was then introduced into this plasmid by blunt-end ligation following SalI digestion and end-filling by Klenow reaction to create the destination vector pFP3FLAGSII. The full-length coding sequence for TIR1 was amplified from an *Arabidopsis* cDNA library using Gateway-compatible primers (see Supplementary Table 1) and incorporated into the Gateway donor vector pDONR207 by BP reaction (Invitrogen). The TIR1 coding sequence was then incorporated into pFP3FLAGSII via a Gateway vector. LR reaction was used to form plasmid pFP3FLAGSII-TIR1. Wild-type *Arabidopsis* plants were subsequently transformed using the floral dip method[32] and homozygous lines with single-site were selected from the T_3 generation. Extracts of 10-day-old *35S::Flag-TIR1* seedlings were made as described previously[6] and used in pull-down assays by combining 2.5 mg of crude extract with 5 μg of biotinylated IAA28 domain II peptide (biotinyl-NH-EVAPVVGWPPVRSSRRN-COOH, synthesized by Thermo Scientific), and 65 μl 50% streptavidin-agarose suspension. The assays were incubated for 1 h at 4 °C with mixing then washed three times for 5 min in extraction buffer (0.15 M NaCl, 0.5% Nonidet P40, 0.1 M Tris-HCl pH 7.5, containing 1 mM phenylmethylsulphonyl fluoride, 1 μM dithiothreitol, 10 μM MG132) containing the appropriate auxin treatment. The final processing of the pull-down assays including electrophoresis and western transfer were performed as described previously[6]. The immunodetection of TIR1/AFB–Flag was performed with a 1:5,000 dilution of anti-Flag 2-peroxidase (HRP) antibody (Sigma) followed by chemiluminescent detection with ECL plus reagents (Amersham).

Transcript profiling. Total RNA was extracted from roots using an RNeasy Plant Micro Kit (Qiagen), including on-column DNase digestion to eliminate genomic DNA from the samples. A 500-ng aliquot of RNA was reverse-transcribed using a Transcriptor First Strand cDNA synthesis kit (Roche) and anchored-oligo (dT)18. Real-time qPCRs were performed on a Roche Light Cycler 480 system using the prevalidated single hydrolysis probes, Sensimix probe master mix (Quantace), and gene-specific primers (see Supplementary Table 1).

31. Friml, J. *et al.* Efflux-dependent auxin gradients establish the apical-basal axis of *Arabidopsis*. *Nature* **426,** 147–153 (2003).
32. Clough, S. J. & Bent, A. F. Floral dip: a simplified method for *Agrobacterium*-mediated transformation of *Arabidopsis thaliana*. *Plant J.* **16,** 735–743 (1998).
33. Rogg, L. E., Lasswell, J. & Bartel, B. A gain-of-function mutation in IAA28 suppresses lateral root development. *Plant Cell* **13,** 465–480 (2001).
34. Cutler, S. R., Ehrhardt, D. W., Griffitts, J. S. & Somerville, C. R. Random GFP:cDNA fusions enable visualization of subcellular structures in cells of *Arabidopsis* at a high frequency. *Proc. Natl Acad. Sci. USA* **97,** 3718–3723 (2000).
35. Karimi, M., De Meyer, B. & Hilson, P. Modular cloning in plant cells. *Trends Plant Sci.* **10,** 103–105 (2005).
36. Levesque, M. P. *et al.* Whole-genome analysis of the SHORT-ROOT developmental pathway in *Arabidopsis*. *PLoS Biol.* **4,** e143 (2006).
37. Barbier de Reuille, P., Bohn-Courseau, I., Godin, C. & Traas, J. A protocol to analyse cellular dynamics during plant development. *Plant J.* **44,** 1045–1053 (2005).
38. Fernandez, R. *et al.* Imaging plant growth in 4D: robust tissue reconstruction and lineaging at cell resolution. *Nature Methods* **7,** 547–553 (2010).
39. Grandjean, O. *et al. In vivo* analysis of cell division, cell growth, and differentiation at the shoot apical meristem in *Arabidopsis*. *Plant Cell* **16,** 74–87 (2004).
40. Holman, T. J. *et al.* Statistical evaluation of transcriptomic data generated using the Affymetrix one-cycle, two-cycle and IVT-Express RNA labelling protocols with the *Arabidopsis* ATH1 microarray. *Plant Methods* **6,** 9 (2010).

41. French, A., Ubeda-Tomas, S., Holman, T. J., Bennett, M. J. & Pridmore, T. High-throughput quantification of root growth using a novel image-analysis tool. *Plant Physiol.* **150,** 1784–1795 (2009).

42. Lohmann, D. *et al.* SLOW MOTION is required for within-plant auxin homeostasis and normal timing of lateral organ initiation at the shoot meristem in *Arabidopsis*. *Plant Cell* **22,** 335–348 (2010).